Orig Life Evol Biosph (2016) 46:247–271
DOI 10.1007/s11084-015-9474-x

ARCHEAN GEOCHEMISTRY

Occurrence of Tourmaline in Metasedimentary Rocks of the Isua Supracrustal Belt, Greenland: Implications for Ribose Stabilization in Hadean Marine Sediments

Shinpei Mishima[1] · **Yoko Ohtomo**[2] · **Takeshi Kakegawa**[1]

Received: 31 March 2015 / Accepted: 30 October 2015 /
Published online: 2 December 2015

Abstract Abiotic formation of RNA was important for the emergence of terrestrial life, but the acknowledged difficulties of generating and stabilizing ribose have often raised questions regarding how the first RNA might have formed. Previous researchers have proposed that borate could have stabilized ribose; however, the availability of borate on the early Earth has been the subject of intense debate. In order to examine whether borate was available on the early Earth, this study examined metasedimentary rocks from the Isua Supracrustal Belt. Garnet, biotite, and quartz comprise the major constituents of the examined rocks. Field relationships and the chemical compositions of the examined rocks suggest sedimentary origin. The present study found that garnet crystals contain a number of inclusions of tourmaline (a type of borosilicate mineral). All tourmaline crystals are Fe-rich and categorized as schorl. Both garnet and tourmaline often contain graphite inclusions and this close association of tourmaline with garnet and graphite has not been recognized previously. Garnet–biotite and graphite geothermometers suggest that the tourmaline in garnet experienced peak metamorphic conditions (~500 °C and 5 kbar). The mineralogical characteristics of the tourmaline and the whole rock composition indicate that the tourmaline formed authigenically in the sediment during diagenesis and/or early metamorphism. Clay minerals in modern sediments have the capability to adsorb and concentrate borate, which could lead to boron enrichment during diagenesis, followed by tourmaline formation under metamorphic conditions. Clay minerals, deposited on the early Archean seafloor, were the precursors of the garnet and biotite in the examined samples. The studied tourmaline crystals were most likely formed in the same way as modern tourmaline in marine sediments. Therefore, boron enrichment by clays must have been possible even during the early Archean. Thus, similar

✉ Shinpei Mishima
mishima.shinpei.t6@dc.tohoku.ac.jp

[1] Department of Earth Science, Tohoku University, Aza-aoba 6-3, Aramaki, Aoba-ku, Sendai, Japan

[2] Faculty, Graduate School and School of Engineering, Hokkaido University, Kita 13, Nishi 8, Kita-ku, Sapporo, Japan

enrichment could have been possible during the Hadean, providing a stabilization agent for ribose.

Keywords Ribose · Borate · RNA · Marine sediments · Early Earth · Isua supracrustal belt

Introduction

The importance of RNA for the emergence of terrestrial life has been widely recognized. Gilbert (1986) envisaged a "RNA world" as a progenitor of the DNA-dominated biology that we know today. However, even the most plausible synthetic route for the formation of ribonucleotide, the monomeric unit of RNA, is far from completely understood (e.g., Orgel 2004; Sutherland 2010; Benner et al. 2012 and references cited therein). Ribonucleotide is composed of ribose, nucleobase, and phosphate, although the availability of ribose in particular for prebiotic reactions is unclear. The formose reaction, the oligomerization of formaldehyde that proceeds in alkaline solutions, is conceivable as a prebiotic process for ribose synthesis. However, ribose is only a minor component in the mixtures of various sugars and hydrocarbons generated through this reaction (Breslow 1959; Shapiro 1988; Orgel 2004; Benner et al. 2012). Furthermore, ribose shows the greatest instability of the aldopentoses during the formose process (Larralde et al. 1995). Based on this experimental evidence, the idea of ribose being an essential component of the primordial genetic material has been challenged, and the formation of alternative polymers instead of RNA has been explored (Nielsen 2007).

Recently, experimental investigations have revealed that ribose can be stabilized via the formation of complexes containing borate (Prieur 2001; Ricardo et al. 2004). This mechanism might possibly provide an intermediate step for the prebiotic synthesis of ribonucleotide. However, problems arise from a geochemical point of view. For ribose stabilization, a high concentration of aqueous borate is required and it has been debated whether such a boron-rich environment was available on the Hadean Earth (Grew et al. 2011; Benner et al. 2012). Some researchers have argued that Hadean alkaline terrestrial lakes could have concentrated boron (Kim et al. 2011; Benner et al. 2012); however, boron-bearing evaporites have not been reported in early to mid-Archean terrains (Grew et al. 2011). Given the lack of primitive Earth landmass exposed to the atmosphere, such an accumulation of boron in a continental environment might have been rare and thus, it would be quite difficult to find in the geological record. Conversely, intense submarine hydrothermal activity did ensure the availability of aqueous borate in the marine environment of that time (Kakegawa et al. 2002; Holm et al. 2006; Holm 2012).

It is well recognized that modern upper oceanic crusts can store a large amount of boron. For example, boron contents reach up to 270 ppm in altered oceanic crust (Leeman and Sisson 1996). Furukawa et al. (2013) suggested that dissolved borate might be abundant in alkaline fluids derived from serpentinization. In addition to the mafic and ultramafic rocks of the oceanic crust, marine sediments behave as good boron reservoirs (i.e., 180 ppm; Leeman and Sisson 1996). Clay minerals can adsorb borate on their surfaces and contribute to the concentration of borate in marine sediments (Henry and Dutrow 1996). Such clay-mediated adsorption processes might have occurred even during the Hadean. Moreover, in addition to borate, organic molecules can be adsorbed onto the surfaces of clay mineral and consequently, exported from the surface to the deep ocean (Kennedy et al. 2002). Therefore, marine sediments might have created an ideal environment for interactions between borate and organic molecules.

The presence of tourmaline (a type of borosilicate mineral) in the Isua Supracrustal Belt (ISB) demonstrates the availability of aqueous borate in the early ocean (Appel 1995; Chaussidon and Appel 1997). Tourmalines have been reported in the ISB from several lithologies, such as metamorphosed volcanic rocks, hydrothermal veins, and metasedimentary rocks (e.g., Appel 1995; Chaussidon and Appel 1997; Grew et al. 2015). Previous investigators have reported the occurrence of tourmaline in garnet–biotite schist, the precursor of which was most likely clay-rich marine sediments. In particular, Grew et al. (2015) described the details of tourmaline in various rocks in the ISB and they proposed the presence of authigenic tourmaline in a ca. 3.7 Ga "proto-arc" sedimentary basin. However, questions exist regarding whether the precursors of previously examined garnet–biotite schists were metasedimentary rocks or metasomatized volcanic rocks (Rosing et al. 1996). Therefore, it has been desirable to accumulate further geological evidence regarding the sedimentary origin of the Isua tourmaline, in order to constrain both the early Archean boron cycle in general and the hydrosphere to lithosphere flux in particular.

Recently, rocks of obvious sedimentary derivation containing biogenic graphite have been reported from the ISB (Rosing 1999; Ohtomo et al. 2014). Detailed mineralogical studies of these rocks could provide insight into the 3.8–3.7 Ga ocean chemistry, particularly with regard to the presence of borate. Thus, in this study, the Isua meta-sedimentary rocks were examined to both ascertain the presence of tourmaline and determine whether boron-rich environments were present in the early Archean surface environments.

Geologic Setting and Samples

The ISB in southwestern Greenland is part of the Itsaq Gneiss Complex. Rocks of the ISB consist mainly of Eoarchean metavolcanics and minor metasedimentary rocks (e.g., Furnes et al. 2007, 2009) (Fig. 1a). It is thought that both ~3.8 Ga southern and ~3.7 Ga northern juvenile crustal complexes were tectonically juxtaposed along mylonite zones during the Eoarchean, which is supported by U–Pb zircon dating (Nutman et al. 2009, 2013). Most of the ISB was strongly deformed by Eoarchean tectonism (Nutman et al. 2013) and converted into amphibolite metamorphic facies. Nevertheless, rocks in the northwestern area of the ISB generally represent lower strain and lower metamorphic grade (Nutman and Bridgwater 1986). This low-strain zone is often subdivided into: (1) garbenschiefer amphibolite and (2) undifferentiated amphibolite (Furnes et al. 2009). The garbenschiefer amphibolite occupies the central portion of the northwestern ISB and it consists of tholeiitic to boninitic metabasic rocks with relict pillow structures, volcanoclastic metasediments, and banded iron formations (BIFs). The undifferentiated amphibolite is characterized by dominant metavolcanic amphibolites with metasomatized rocks, with minor BIFs and siliceous rocks.

The sampling locality for the present study lies in the garbenschiefer amphibolite in the western part of the ISB, which is about 1 km west of the location of a Bouma sequence (Rosing 1999; Fig. 1b). Metabasalts occupy a large part of the sampling area. Three layers of BIFs are concordantly intercalated with metabasalts. Notable units include graphite-rich schists and garnet–biotite schists, with biogenic graphite previously reported in the former (Ohtomo et al. 2014). Rock samples were collected from an outcrop of the garnet–biotite schist. This outcrop is sandwiched between the garbenschiefer amphibolite at its western end and BIFs at its eastern end, dipping vertically and concordant with the BIFs. The thickness of the outcrop is approximately 5 m. The outcrop is considered part of the unit described by Ohtomo et al. (2014). Five samples (sample numbers: 3071908, 5081204, 5081205, 5081206, and 5081207)

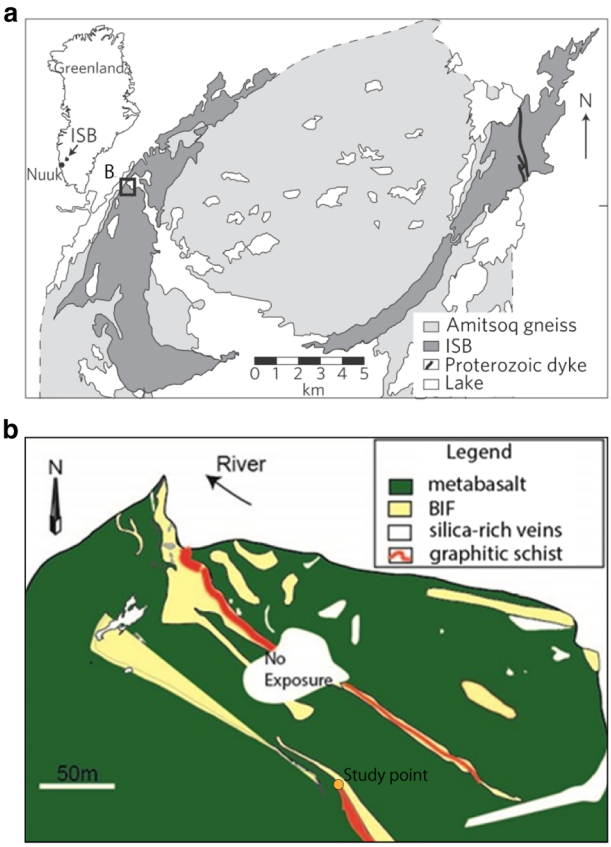

Fig. 1 **a** Location of ISB. **b** Geologic map of the study area (modified from Ohtomo et al. (2014))

from this outcrop were examined in the present study. In addition to analyses of the garnet–biotite schists, tourmalines from the quartz vein in the ISB were also examined (Appel et al. 2001) and their chemical compositions analyzed for comparison.

Analytical Methods

Major and Trace Element Composition Analysis

Major and trace element compositions were determined from powdered bulk rock samples using Inductively Coupled Plasma Mass Spectroscopy (ICP–MS). The analyses were performed by a commercial company (Activation Lab, 1336 Sandhill Drive, Ancaster, Ontario, Canada) under research-quality conditions.

SEM and EPMA Analyses

Samples were examined using an S-3400 scanning electron microscope (SEM; HITACHI, Tokyo, Japan) using a back-scattered electron detector (BSE) at Geosciences Department of Tohoku University, to examine the textural relationships among the minerals. Chemical

compositions of the minerals were determined using a JXA-8800 M (JEOL, Tokyo, Japan) and a wavelength dispersive spectrometer (WDS) at Geosciences Department of Tohoku University. All analyses were performed with an accelerating voltage of 15 kV and beam current of 15 nA.

Laser Raman Microspectroscopy

Laser Raman microspectroscopy was performed on minerals using an NRS-5100 device (JASCO, Tokyo, Japan) at School of Engineering of Tohoku University. The diameter of the laser diode, input power, delivered power to the sample surface, and acquisition time for each spectrum were 532.92 nm, 50 mW, 3.3 mW, and 40 s, respectively. Peak position, band area (i.e., integrated area), full width at half maximum (FWHM), and Gaussian fittings of the bands were determined using the software provided with the NRS-5100 device.

Results

Sample Petrography

The major minerals in the examined schists are garnet, biotite, muscovite, and quartz (Fig. 2). Typically, garnets range in diameter from 0.5 to 1 mm. Garnets show poikiloblastic textures with small inclusions of quartz and biotite (Fig. 2b). In addition, pyrite and ilmenite are also present in the garnet as accessory minerals. Biotite (~0.1-mm diameter) often surrounds the garnet crystals. Garnet and biotite compositions are dominated by the iron end-member components of almandine and annite, respectively (Table 1). Tourmalines are mainly found as inclusions in the garnet (Fig. 2c). The details of the tourmaline textures and compositions are described in Tourmaline Section.

Whole-Rock Compositions

The results of the whole rock analyses are presented in Table 2. The SiO_2 and Al_2O_3 contents in the studied samples range from 56.45 to 63.78 wt.% and from 10.94 to 14.66 wt.%, respectively. Notably, Fe_2O_3 contents are relatively high (11.77–19.98 wt.%) compared with typical pelitic or metapelitic rocks of younger ages. Generally, Cr and Ni concentrations are high, probably because of inputs from mafic components. However, Zr concentrations, which might be derived from felsic components, range from 66 to 98 ppm, indicating high concentrations of these components. All samples have moderate to high total rare earth element (REE) concentrations. Concentrations of chalcophile elements (Cu, Zn, Pb) are not significantly high.

Tourmaline

A photomicrograph of tourmaline is shown in Fig 3a. Tourmalines in the garnet–biotite schists were euhedral and showed small grain sizes (<50-μm diameter perpendicular to the c-axis). No strong color zonation from core to rim was visible (Fig. 3a). Most of the tourmaline grains were included within garnet crystals and the tourmaline itself contained tiny inclusions, such as graphite, quartz, and ilmenite (Fig. 3a).

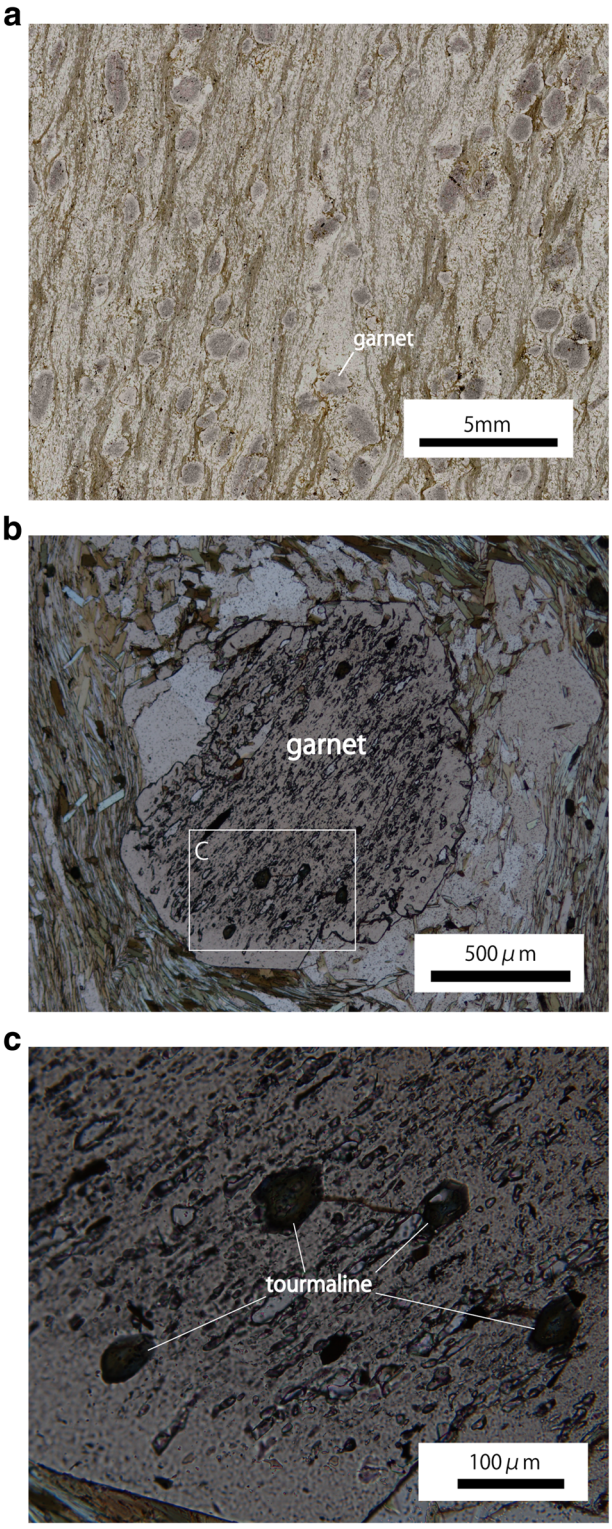

Fig. 2 **a** Thin section photograph of one of the examined samples. **b** Photomicrograph of garnet in garnet–biotite schist, showing poikiloblastic texture. Area marked by "C" corresponds to Fig. 2(c). **c** Garnet with tourmaline inclusions. Both (**b**) and (**c**) were taken with plane-polarized light

Table 1 Representative analyses of garnet and biotite in the garnet–biotite schists from the ISB

	Garnet		Biotite		
	Core	Rim	Inclusion	Rim	Matrix
SiO_2	36.93	36.61	35.20	34.34	34.72
Al_2O_3	20.75	20.69	18.41	18.62	18.52
TiO_2	0.00	0.00	1.83	1.73	1.65
FeO[1]	36.42	39.18	23.98	25.71	26.31
MnO	1.29	1.35	0.00	0.00	0.00
MgO	1.09	1.15	7.25	6.12	6.13
CaO	3.68	0.95	0.00	0.00	0.00
Na_2O	0.00	0.00	0.18	0.13	0.11
K_2O	0.00	0.00	9.52	9.55	9.36
total	100.15	99.94	96.38	96.18	96.78
Si	6.003	5.999	5.422	5.357	5.384
Al	3.974	3.997	3.343	3.424	3.385
Ti	0.000	0.000	0.213	0.202	0.192
Fe	4.950	5.370	3.090	3.354	3.412
Mn	0.177	0.188	0.000	0.000	0.000
Mg	0.265	0.282	1.664	1.422	1.416
Ca	0.641	0.167	0.000	0.000	0.000
Na	0.000	0.000	0.055	0.039	0.032
K	0.000	0.000	1.871	1.900	1.852
Oxygens	24	24	22	22	22

Tourmaline is a borosilicate mineral, characterized by its complex chemical composition with a generalized structural formula of $XY_3Z_6(T_6O_{18})(BO_3)_3V_3W$. The nine-fold coordinated X-site is occupied by Na^+, Ca^{2+}, K^+, or is vacant. Y and Z are both octahedral sites, but differ in their capacity for cations. The Y-site can incorporate diverse multivalent cations, such as Li^+, Mg^{2+}, Fe^{2+}, Mn^{2+}, Al^{3+}, Fe^{3+}, Mn^{3+}, or Cr^{3+}, whereas the Z-site is typically occupied by Al^{3+} but it may also be occupied by Mg^{2+}, Fe^{3+}, Cr^{3+}, or V^{3+}. The V-site is typically occupied by OH^- but it may also be occupied by O^{2-}, and the W-site is occupied by O^{2-}, OH^-, or F^{2-} (e.g., Henry et al. 2011). The results of tourmaline analyses by WDS are shown in Table 3. As WDS cannot analyze light elements such as H, and Li, or determine the valence state of transition metals, and as B requires a special analyzing crystals and setup, the following assumptions were made in order to calculate the structural formula of tourmaline: (1) B fully occupies the triangular B sites, which results in a stoichiometric constraint of B=3 atoms per formula unit (apfu). This is likely to be valid for the vast majority of tourmalines, because boron fully occupies the B site with no tetrahedrally coordinated B (Clark 2007). (2) The sum of the T + Z + Y cations is set to equal 15. This procedure is recommended for calculating a formula for tourmaline with low Li contents and minor B in the tetrahedral sites (Henry et al. 2011). Because tourmalines that coexist with minerals such as biotite and muscovite contain small to insignificant amounts of Li because of preferential partitioning of Li into those coexisting phases (Henry and Dutrow 1996), this assumption should apply reasonably well to metamorphic tourmaline. (3) OH + F is fixed by the total cationic charge (Henry et al. 2011)

Table 2 Major (wt%) and trace element (ppm) compositions of garnet–biotite schists from the ISB

	Garnet–biotite schists					
	3071908	5081204	5081205	5081206	5081207	Average
wt%						
SiO_2	59.47	56.45	61.56	63.12	63.78	60.88
Al_2O_3	10.94	14.07	13.54	14.66	12.91	13.23
Fe_2O_3	19.98	12.13	14.53	11.77	14.66	14.62
MnO	0.47	0.14	0.22	0.13	0.16	0.23
MgO	3.18	2.75	2.61	1.76	1.43	2.35
CaO	0.8	2.92	0.17	0.08	0.12	0.82
Na_2O	0	1.44	0.1	0.1	0.31	0.39
K_2O	1.29	4.48	4.07	5.24	4.74	3.97
TiO_2	0.32	1.51	0.5	0.58	0.52	0.69
P_2O_5	0.02	0.14	0.04	0.03	0.04	0.06
LOI	3.55	4	2.67	2.52	1.34	2.82
ppm						
Be	0	2	2	4	4	2.4
Sc	15	26	27	18	20	21.2
V	74	265	126	107	114	137.2
Cr	343	40	490	370	440	336.6
Co	27	21	25	14	21	21.6
Ni	121	49	195	155	146	133.2
Cu	11	335	1	14	<1	72.2
Zn	89	117	86	127	76	99
Ga	14	23	15	18	14	16.8
Ge	10.3	3	8	9	12	8.46
Rb	79	157	144	190	201	154.2
Sr	5	50	10	14	12	18.2
Y	12.2	18	11	13	12	13.24
Zr	66	93	68	97	76	80
Nb	1.9	4	2	3	3	2.78
Ag	0	0.7	0.6	0.8	0.8	0.58
Cs	4.3	5.7	5.7	8.4	9.4	6.7
Ba	30	160	97	152	107	109.2
La	10.7	11.6	5.4	9.3	8.1	9.02
Ce	20.3	26.3	11.9	18	13.9	18.08
Pr	2.4	3.59	1.35	2.38	2.1	2.37
Nd	10.2	14.9	5.6	9.6	8.6	9.78
Sm	2.36	3.5	1.3	2.1	1.9	2.24
Eu	0.944	0.98	0.49	0.83	0.75	0.8
Gd	2.45	3.3	1.3	1.9	1.8	2.15
Tb	0.37	0.6	0.2	0.3	0.3	0.36
Dy	1.96	3.3	1.6	1.8	1.9	2.12
Ho	0.38	0.6	0.3	0.4	0.4	0.42
Er	1.1	1.8	1	1.2	1.3	1.28

Table 2 (continued)

	Garnet–biotite schists					
	3071908	5081204	5081205	5081206	5081207	Average
Tm	0.16	0.26	0.15	0.18	0.2	0.19
Yb	1.02	1.6	1	1.1	1.3	1.21
Lu	0.144	0.23	0.14	0.17	0.19	0.18
Hf	1.9	2.9	2.1	2.9	2.3	2.42
Ta	0.25	0.3	0.2	0.2	0.2	0.23
Tl	0.23	0.4	0.4	0.5	0.6	0.43
Pb	14	12	8	8	9	10.2
Th	1.56	1.3	1.3	2.1	1.5	1.56
U	0.4	0.4	0.3	0.6	0.4	0.42

and calculated. (4) Tetrahedral Al^{3+} is assigned to the Z-site first and in the case of complete Z-site occupancy, the remaining Al^{3+} is assigned to the Y-site.

Compositions of tourmaline in the garnet–bioitite schists were plotted in terms of the X- and Y-site occupancies (Fig. 4a and b). The compositions of the tourmalines from the quartz vein in the ISB were also analyzed in this study and they are plotted for comparison. Figure 4a shows that all tourmalines belong to the alkali group. Considering their Y-site occupancy, the examined tourmalines are classified as schorl (Fig. 4b). To identify the tourmalines further, Raman spectroscopic analyses were performed. Figure 5 shows a Raman spectrum of the tourmaline from the garnet–biotite schists. In this study, the focus was on the spectral range of 300–1600 cm^{-1}, which covers the metal-ion oxygen bonding vibrations (Hoang et al. 2011). Peaks that lie between 800 and 110 cm^{-1} can be assigned to modes that include B–O, Si–O, O–Al–O motion, BO_3 breathing, Al–O stretching, as well as AlO_6 and BO_3 deformations. The most intense band at ~600–800 cm^{-1} is generated by the symmetrical Si–O–Si vibration. The peaks at 400–600 cm^{-1} are due to Al–O and Y–O bond stretching (Y: cations occupying the Y-sites), while those at <400 cm^{-1} arise mainly from X–O bond stretching (X: cations occupying the X-sites). The poor resolution of both spectra is attributed to the occupation of the Y-sites by several cations such as Al, Mg, and Fe (Hoang et al. 2011). Compared with almost all other tourmalines found in other parts of the ISB, the tourmalines investigated in the present study have greater Fe enrichment. The significance of this Fe enrichment of the tourmaline is discussed in Origin of Tourmaline Section.

Graphite

Graphite grains were found as inclusions in the garnet, some of which were very close to or were included in the tourmaline. Raman spectra of the graphite in the garnet–biotite schists, as well as in the tourmaline, were also obtained and the Raman shift data are summarized in Fig. 6. Well-ordered graphite shows several bands in its Raman spectrum, including the first-order G band located at ~1582 cm^{-1}, which can be attributed to C–C vibrations of aromatic carbon (Beyssac et al. 2002). If a carbonaceous material is disordered to some extent, it generally displays additional first-order bands designated as D bands. These D bands are located at ~1355 cm^{-1} (D1 band), ~1550 cm^{-1} (D3 band), and ~1620 cm^{-1} (D2 band). In the case of even further disordered matter, an additional second-order band can be seen at

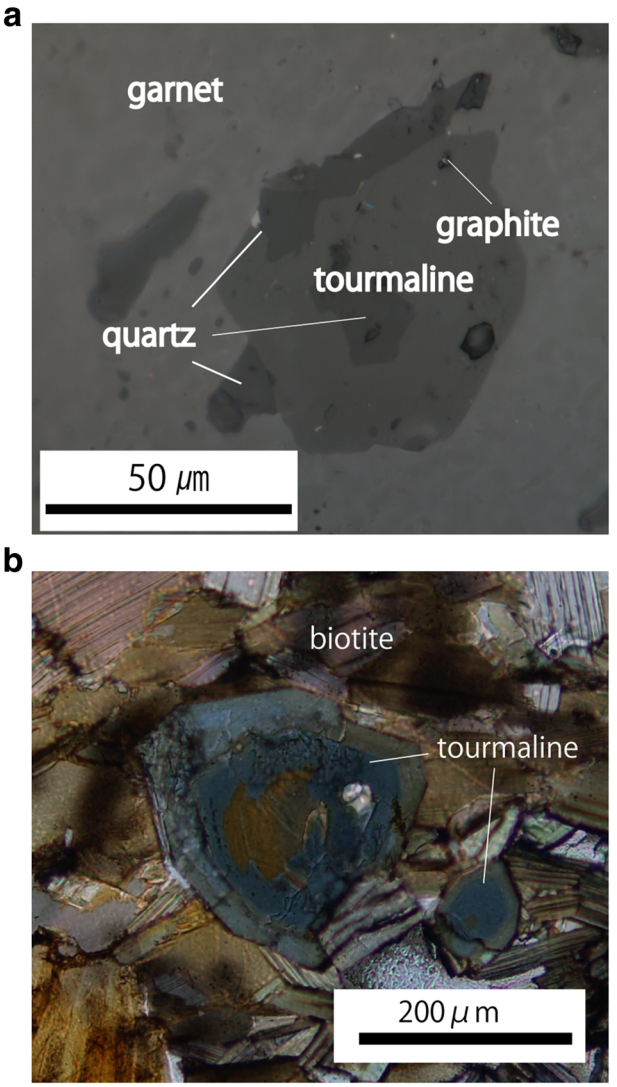

Fig. 3 Photomicrographs of tourmaline in garnet–biotite schist (**a**) and quartz vein (**b**) in the ISB. Both (**a**) and (**b**) were taken with plane-polarized light. Tourmaline in the garnet–biotite schist, which is surrounded by garnet, has small inclusions of quartz and graphite and shows no distinctive color zonation. Tourmaline in quartz vein shows strong color zonation from core to rim

~2900 cm^{-1}. The 1050–1850 cm^{-1} region of the example Raman spectrum, obtained from the grain shown in Fig. 3a, includes all the first-order bands and clearly shows the presence of sharp G and D1 bands (Fig. 6); the G2 band appears on the shoulder of the G band (Fig. 6).

Discussion

Sources of Sediments

Figure 7 shows the REE patterns of the examined samples. Chondrite-normalized REE patterns display relative enrichment of light REEs (LREEs) compared with heavy REEs (HREEs) (Fig. 7a). Overall, the REE patterns of the examined rocks are similar to modern

Table 3 Selected analyses of tourmalines in the garnet–biotite schists and quartz vein from the ISB

Garnet–Biotite Schists												Quartz Vein			
Grain	1	3	4	5	7	8	9	10	12	14	18	21 (core)	21 (rim)	22 (core)	22 (rim)
wt%															
B_2O_3 (calc)	10.18	10.40	10.38	10.41	10.25	10.43	10.30	10.33	10.30	10.36	10.44	10.22	10.49	10.36	10.61
SiO_2	35.29	36.03	36.01	36.37	34.84	35.30	35.55	36.27	35.39	35.21	35.22	35.47	36.33	35.68	36.43
Al_2O_3	31.10	32.70	31.37	31.84	31.89	33.42	33.00	32.14	32.18	32.20	33.29	30.85	31.56	30.69	32.59
TiO_2	0.45	0.28	1.00	0.59	0.88	0.19	0.29	0.22	0.40	0.75	0.46	0.42	0.40	0.32	0.47
Cr_2O_3	0.14	0.24	0.24	0.20	0.30	0.22	0.20	0.18	0.24	0.21	0.21	0.49	0.13	0.33	0.13
FeO	12.05	11.19	11.40	11.11	10.72	11.42	11.66	10.67	11.23	12.13	11.88	10.07	7.62	8.31	8.08
MgO	3.64	3.67	4.11	4.05	4.17	3.68	2.93	3.86	3.83	3.59	3.49	4.86	6.88	6.76	6.38
CaO	0.73	0.00	0.19	0.17	0.84	0.00	0.46	0.19	0.79	0.69	0.98	0.80	0.84	1.64	1.03
Na_2O	1.60	2.12	2.04	1.73	1.78	1.60	1.42	1.86	1.50	1.66	1.17	1.99	2.07	1.64	1.74
H_2O (calc)	3.31	3.35	3.34	3.40	3.24	3.67	3.30	3.26	3.33	3.40	3.49	3.20	3.37	3.31	3.40
F	0.00	0.00	0.00	0.00	0.00	0.00	0.00	0.00	0.00	0.00	0.00	0.00	0.00	0.00	0.00
Cl	0.00	0.00	0.00	0.00	0.00	0.00	0.00	0.00	0.00	0.00	0.00	0.00	0.00	0.00	0.00
total	98.49	99.98	100.08	99.87	98.91	99.93	99.11	98.98	99.19	100.20	100.63	98.37	99.69	99.04	100.86
Formulas normalized to T + Y + Z = 15															
B	3.000	3.000	3.000	3.000	3.000	3.000	3.000	3.000	3.000	3.000	3.000	3.000	3.000	3.000	3.000
Si	6.023	6.019	6.030	6.072	5.905	5.880	6.000	6.100	5.970	5.910	5.860	6.030	6.020	5.990	5.970
TAl	0.000	0.000	0.000	0.000	0.095	0.120	0.000	0.000	0.030	0.090	0.140	0.000	0.000	0.010	0.030
T-site Total	6.023	6.019	6.030	6.072	6.000	6.000	6.000	6.100	6.000	6.000	6.000	6.030	6.020	6.000	6.000
Al	6.256	6.437	6.192	6.267	6.275	6.440	6.560	6.370	6.370	6.280	6.390	6.180	6.160	6.060	6.260
Ti	0.059	0.035	0.125	0.074	0.112	0.020	0.040	0.030	0.050	0.090	0.060	0.050	0.050	0.040	0.060
Cr	0.019	0.032	0.031	0.026	0.040	0.030	0.030	0.020	0.030	0.030	0.030	0.070	0.020	0.040	0.020
Fe	1.721	1.563	1.596	1.552	1.520	1.590	1.640	1.500	1.580	1.700	1.650	1.430	1.060	1.170	1.110
Mg	0.925	0.914	1.026	1.009	1.053	0.910	0.740	0.970	0.960	0.900	0.870	1.230	1.700	1.690	1.560
Y, Z-site Total	8.978	8.981	8.970	8.928	9.000	9.000	9.000	8.900	9.000	9.000	9.000	8.970	8.980	9.000	9.000
Ca	0.134	0.003	0.034	0.031	0.153	0.010	0.080	0.030	0.140	0.120	0.170	0.150	0.150	0.290	0.180
Na	0.530	0.687	0.662	0.559	0.583	0.520	0.470	0.610	0.490	0.540	0.380	0.660	0.670	0.530	0.550
X-site Total	0.663	0.690	0.695	0.590	0.736	0.530	0.550	0.640	0.630	0.670	0.550	0.800	0.810	0.830	0.730

Table 3 (continued)

Garnet–Biotite Schists												Quartz Vein			
Grain	1	3	4	5	7	8	9	10	12	14	18	21 (core)	21 (rim)	22 (core)	22 (rim)
F	0.000	0.000	0.000	0.000	0.000	0.000	0.000	0.000	0.000	0.000	0.000	0.000	0.000	0.000	0.000
Cl	0.000	0.000	0.000	0.000	0.000	0.000	0.000	0.000	0.000	0.000	0.000	0.000	0.000	0.000	0.000
OH	3.769	3.737	3.736	3.791	3.666	4.084	3.718	3.663	3.750	3.809	3.872	3.631	3.724	3.706	3.725
V, W-site Total	3.769	3.737	3.736	3.791	3.666	4.084	3.718	3.663	3.750	3.809	3.872	3.631	3.724	3.706	3.725
X-site vacancy	0.336	0.310	0.304	0.410	0.264	0.470	0.450	0.360	0.370	0.340	0.450	0.190	0.180	0.180	0.270
Mg/(Mg + Fe)	0.350	0.369	0.391	0.394	0.409	0.364	0.311	0.393	0.378	0.346	0.345	0.462	0.616	0.591	0.584
Tourmaline species	Sc	Sc	Sc	Sc	Sc	Sc	Sc	Sc	Sc	Sc	Sc	Sc	Dv	Dv	Dv

All Fe measured as FeO. *Sc* Schorl, *Dv* Dravite

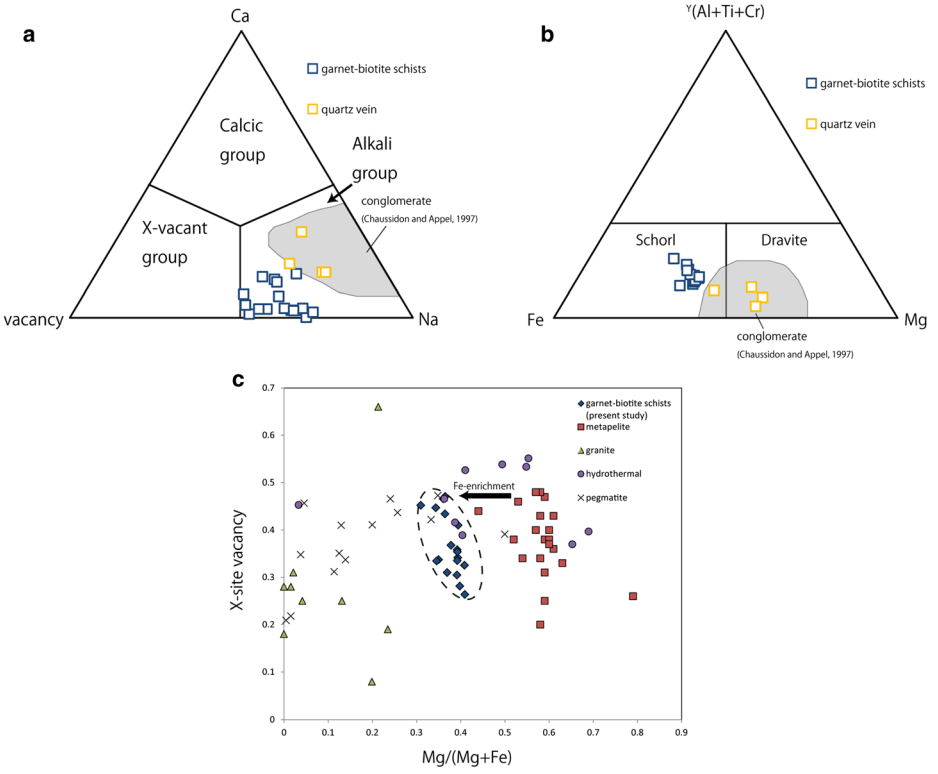

Fig. 4 **a** and **b** Compositional plots of tourmaline in garnet–biotite schist and quartz vein from the ISB for X- and Y-site occupancy. Compositional fields and lines are labeled for species according to Henry et al. (2011). *Gray* shaded area represents the compositional range of tourmalines from a conglomerate in the ISB according to Chaussidon and Appel (1997). The compositions of tourmaline in garnet-biotite schist occupy the distinct area from those in quartz vein (this study) and conglomerate (from literatures). This indicates that they have different origins. **c** Plot of Mg/(Mg + Fe) content vs. X-site vacancy for various types of tourmaline. Tourmaline compositions, except those of the garnet–biotite schists, were compiled from Kawakami and Ikeda (2003) (Phanerozoic metapelites), Trumbull et al. (2008) (granite), Williamson et al. (2000) (hydrothermal), and Keller et al. (1999) (pegmatite)

sedimentary rocks whose protolith is continental crust. Compared with the examined samples, the REE patterns of the garbenschiefer amphibolite show less enrichment of LREEs and generally flatter element patterns. In addition, Al_2O_3 and Zr concentrations of the examined samples are much higher than those of the garbenschiefer amphibolite and comparable with those of other metasediments with absent Eu-anomalies from the ISB (14.06 wt.% and 112 ppm on average; Bolhar et al. 2005), indicating that the garnet–biotite schists were originally sedimentary rocks. The examined garnet–biotite schists are well laminated and their strikes and dips are concordant with the surrounding BIFs. Such geological occurrence also supports the sedimentary origin of the examined samples.

The post-Archean Australian Shale (PAAS)-normalized REE patterns (Taylor and McLennan 1985) show that the LREE and HREE contents of the garnet–biotite schists are considerably lower than those of the PAAS (Fig. 7b). This depletion of trace elements might be attributable to a difference in source materials relative to the PAAS, because it is believed that the Eoarchean continental crust was less differentiated than the crust of subsequent ages

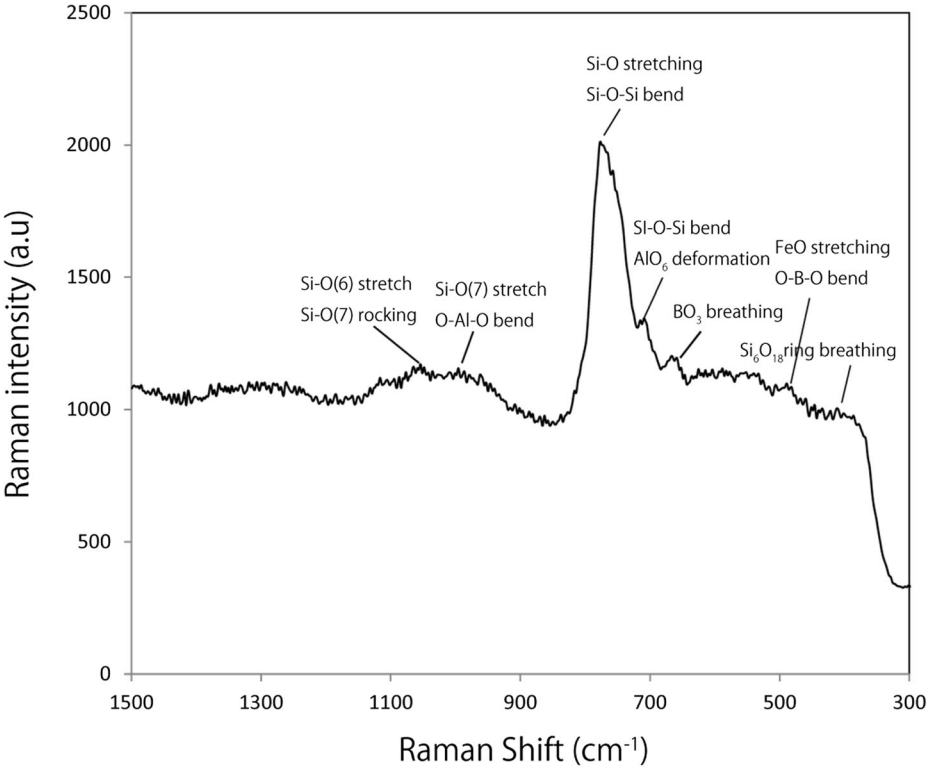

Fig. 5 Raman spectrum of tourmaline in the garnet–biotite schists. Each type of vibration mode is assigned to peaks according to Hoang et al. (2011)

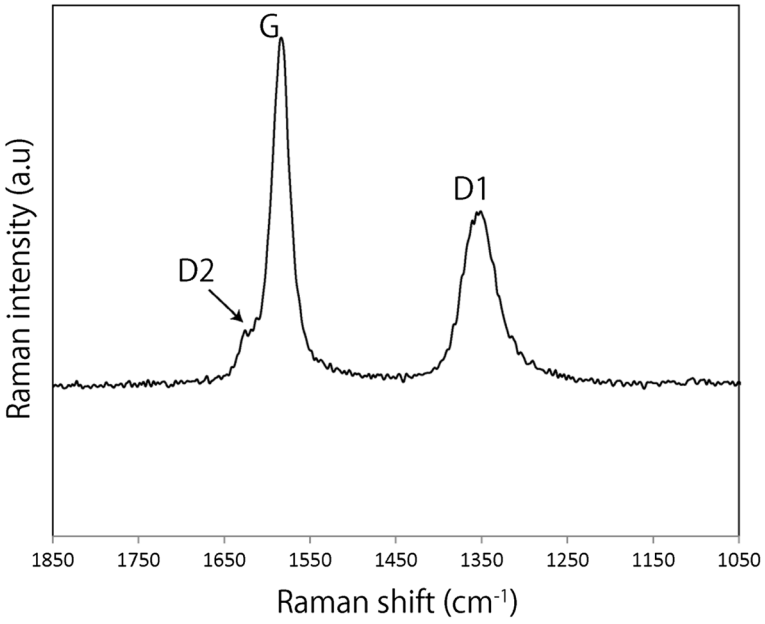

Fig. 6 Raman spectrum of graphite in the garnet–biotite schists

(Bolhar et al. 2005). In addition, the positive Eu anomaly, seen in Fig 7b, might be attributable to coprecipitation of REEs with Fe-minerals derived from submarine hydrothermal plumes. This inference is supported by the observation that Eu was enriched in the Archean seawater because of hydrothermal input into a largely anoxic ocean (Danielson et al. 1992) and elevated abundances of Fe in the examined rocks.

Figure 8a shows the relationship between MgO and FeO of the examined samples. Overall, the Phanerozoic metapelites, North American Shale Composition (NASC), and PAAS show good correlation between FeO and MgO. However, the examined schist samples have higher FeO concentrations compared with the post-Archean samples. Because the examined outcrop was spatially associated with BIFs, Fe-minerals that precipitated from submarine hydrothermal plumes are likely to have contributed some fraction of the Fe in the examined rocks. These whole-rock characteristics of the major and trace elements indicate a sedimentary origin for the protolith of the examined schists, created via the supply of crustal materials from a wide range of lithologies in combination with submarine hydrothermal inputs.

To assess the extent of post-depositional processes on element mobility, a comparison of the relatively immobile and highly mobile elements was performed (Fig. 8b). Although Th and U are usually both enriched in the crust because of igneous differentiation, U is more easily concentrated in a fluid phase during metamorphic dehydration than Th, which results in a rise of the Th/U ratio (Rudnick and Presper 1990). Similarly, K and Rb are also affected by fluid-driven mass transfer, but they would behave differently because of their mobility differences (Bolhar et al. 2005). Thus, if sediment-derived rocks are affected by post-sedimentary hydrothermal alteration or metamorphism, the K/Rb ratio becomes variable in comparison with unaffected rocks. In a plot of Th/U vs. K/Rb (Fig. 8b), data obtained for the present study occupy the same area as other sedimentary rocks. This implies that the examined schists were relatively little affected by fluid-related mass transfer. These geochemical characteristics indicate that the sediment source included both clastic materials (crustal components) and Fe-rich minerals (submarine hydrothermal components), and that elemental abundances, including the elements forming tourmaline, were not disturbed to any significant extent by post-depositional processes. Thus, boron appears to have been primarily incorporated into the sediments and not introduced or removed during metamorphism.

Origin of Tourmaline

Recently, it has been argued that the northern terrane of the ISB formed at an intra-oceanic convergent plate boundary as a “proto-arc” at ~3.7Ga (Nutman et al. 2015). The protolith of the garbenschiefer amphibolite was deposited through the tectonics at that time and clastic material was supplied from neighboring juvenile crust. During transport to the seafloor, large portions of detritus were converted into clay minerals, which are capable of adsorbing borate from ambient seawater, even if only trace amounts of borate are available. Such boron enrichment by clay minerals is a common process in modern marine sediments (Williams et al. 2001) and a similar process may have occurred during the Eoarchean. Subsequent diagenesis led to a release of boron during clay mineral destabilization and breakdown (Henry and Dutrow 1996). This was followed by tourmaline formation because of the low solubility of tourmaline under metamorphic conditions (Henry and Dutrow 1996). Further metamorphism converted clay minerals into biotite, followed by formation of garnet, which incorporated tourmaline. Organic matter, which can also be adsorbed onto the surfaces of clay minerals, was graphitized during metamorphism and partially included in the garnet and

tourmaline. Thus, the coexistence of tourmaline and graphite in the examined metasediments suggests that borate and organic molecules both accumulated in the original sediments.

The occurrence of tourmaline in metasedimentary rocks indicates that tourmaline formed authigenically through diagenesis and early metamorphism, as illustrated above. However, it must be elucidated where and how the tourmaline really formed, because of the possibility of the local hydrothermal or detrital origin of the tourmaline. In the ISB, non-sedimentary and hydrothermal tourmalinite has previously been reported (Appel 1995; Chaussidon and Appel 1997). Moreover, Phanerozoic metasediments commonly contain detrital tourmaline (Henry and Guidotti 1985; Henry and Dutrow 1992). Figure 3b shows a photomicrograph of sea-floor hydrothermal tourmaline taken from the same outcrop as described in Appel et al. (2001). This hydrothermal tourmaline exhibits strong color zonation. Detrital tourmaline in metasediments usually shows metamorphic overgrowths expressed as a compositionally and optically distinctive zonation from core to rim (Henry and Dutrow 1992). However, these features are not observed in tourmalines from the examined garnet–biotite schists (Fig. 3a). This is consistent with the fact that Grew et al. (2015) found no clear detrital cores in the metamorphic tourmaline from the ISB metasediments, indicating that boron was not supplied directly to the original sediments as tourmaline detritus.

X-site vacancy in tourmaline is indicative of the metamorphic grade of a tourmaline's host rock (Henry and Dutrow 1996, 2012). The X-site vacancy of tourmalines in the examined rocks is consistent with medium-grade metamorphism. Furthermore, the tourmalines are enriched in Fe compared with Phanerozoic metasedimentary tourmalines. Such Fe-enrichment possibly reflects the composition of the host rock, which included BIF components (Fig. 7d). These lines of evidence strongly support an authigenic origin of the examined tourmalines, both during diagenesis and early metamorphism.

Grew et al. (2015) recently suggested that the concentration of boron, necessary for the generation of abundant tourmalines in the ISB, might have been localized to a partially isolated basin associated with a proto-arc. Under this scenario, the occurrence of tourmaline from the ISB metasediments might not reflect the widespread presence of borate in the Eoarchean Ocean. The geological survey of this study suggests synchronized sedimentation of BIFs and precursors of the garnet–biotite schist (most likely black shale). In order to form BIFs, significant amounts of Fe and Si must have been transported from distance from deep submarine hydrothermal systems (such a system is also illustrated in Fig. 13 of Grew et al. (2015)). Although the data are not conclusive, we suggest that because the precursors to the garnet-biotite schists analyzed in this study are associated with BIF. The sedimentary basin in which these precursors were deposited is more likely to have been open to deep ocean.

Timing of Tourmaline Formation

The entire ISB was affected by several metamorphic events at different ages. The main metamorphic event in the northwestern part of the ISB, where the study area is located,

Fig. 7 CI chondrite-normalized (**a**) and PAAS-normalized REE patterns (**b**) for the garnet–biotite schists. Normalizing values (mean CI chondrite or PAAS) are from McDonough and Sun (1995), and Taylor and McLennan (1985), respectively. The BIF value in this figure represents the average composition of BIF samples from the northern section (Fig. 1b; Ohtomo et al. 2014). The overall characteristics of these patterns probably reflect the source rocks (see text for further discussion)

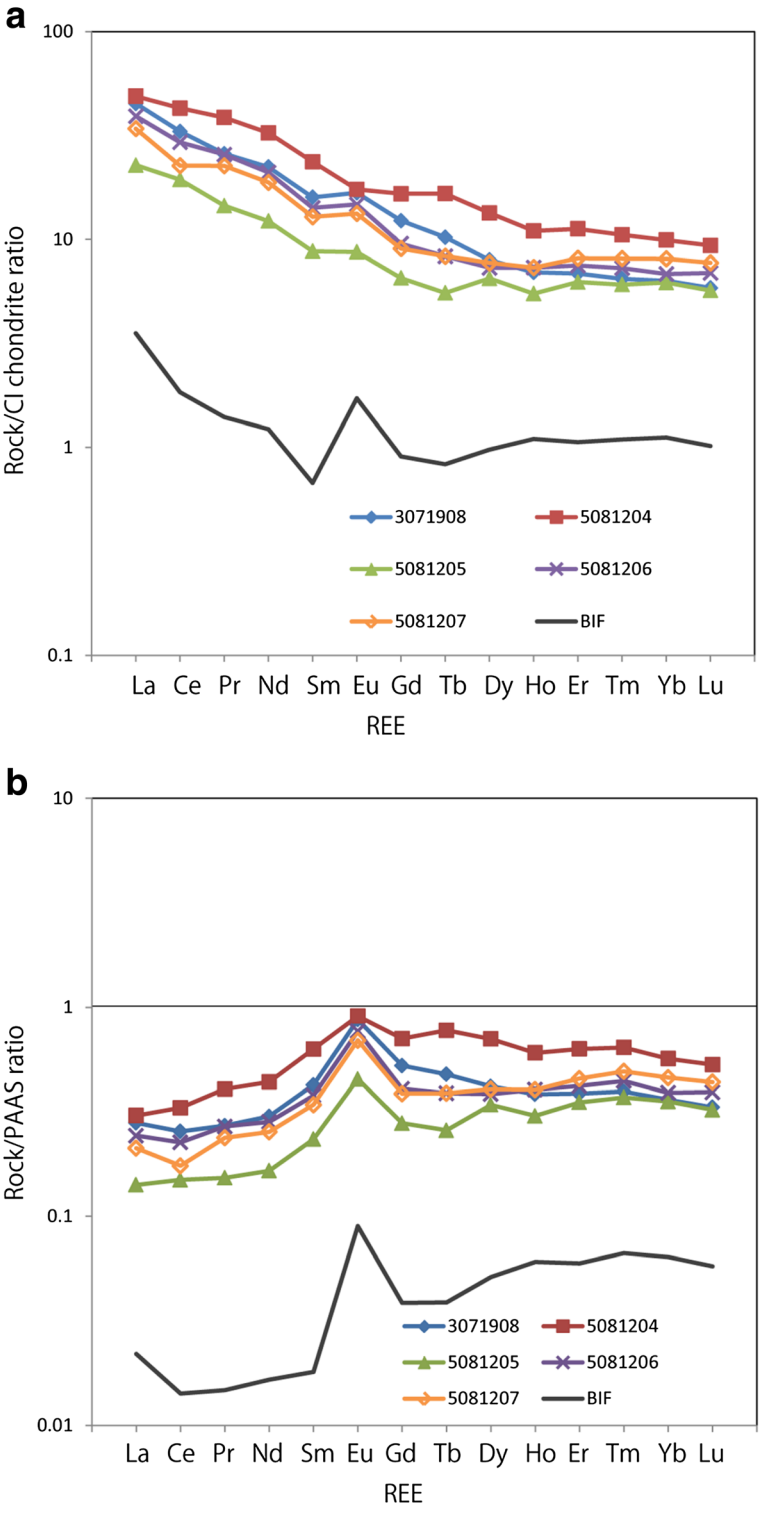
a
100
10
1
0.1
Rock/CI chondrite ratio
3071908
5081204
5081205
5081206
5081207
BIF
La Ce Pr Nd Sm Eu Gd Tb Dy Ho Er Tm Yb Lu
REE
b
10
1
0.1
0.01
Rock/PAAS ratio
3071908
5081204
5081205
5081206
5081207
BIF
La Ce Pr Nd Sm Eu Gd Tb Dy Ho Er Tm Yb Lu
REE

Fig. 8 **a** Plots of MgO vs. FeO content of the garnet–biotite schists, Phanerozoic metapelites (Nakano and Nakamura 2001), and post-Archean shales. The compositional trend of Phanerozoic metapelites displays good correlation between MgO and FeO, suggesting control of FeO content by input of crustal material. The lack of such a correlation and Fe-enrichment in the garnet–biotite schists indicate a contribution of additional Fe sources, probably from Fe-rich minerals precipitated from hydrothermal plumes. **b** Plots of Th/U vs. K/Rb ratios of the garnet–biotite schists, as well as post-Archean and Archean shales. The PAAS and NASC compositions were based on data from Taylor and McLennan (1985) and Gromet et al. (1984), respectively. Data for Archean shales were compiled from Feng and Kerrich (1990) (Abititi), Wronkiewicz (1989) (Pongora), and Wronkiewicz and Condie (1987) (Witwatersrand). The compositional field occupied by the garnet–biotite schists (designated as "present study") is outlined by the dotted circle and overlaps with the compositions of most of the other shales, indicating no apparent metasomatic alteration

occurred in the Eoarchean, probably during the 3.66–3.6 Ga Isukasian tectonic event (Nutman et al. 2013). Moreover, there are no geologic indicators that the area received metamorphic overprinting during the Neoarchean. Here, two types of geothermometers were adopted to evaluate the metamorphic effects on the examined samples: (1) a garnet–biotite geothermometer (Ferry and Spear 1978) and (2) a graphite geothermometer (Beyssac et al. 2002). The details of both methods are described in the Appendix. The garnet–biotite geothermometer is the most commonly used method for estimating temperatures during metamorphism. The method makes use of the temperature dependence of the Fe–Mg exchange reaction between the garnet and biotite solid solutions. To obtain temperatures as close as possible to peak metamorphic temperatures, pairs of garnet and biotite with close spatial association were selected and their chemical compositions measured (Tracy and Robinson 1976). A metamorphic pressure of 5 kbar was assumed, as estimated by a previous study (Boak and Dymek 1982). This assumption is valid, because pressure has only a slight effect on the temperature calculated using the geothermometer. The results of the calculations are listed in Tables 4 and 5. The obtained temperatures are 516±35 °C (garnet–biotite) and 505±50 °C (graphite), which are consistent with the conditions during the Eoarchean metamorphism, as determined by previous studies (Boak and Dymek 1982; Hayashi et al. 2000). Since almost all tourmaline grains were included in the garnet, it can be concluded that the tourmalines described in the present study formed during diagenesis or early metamorphism from borate concentrated in Eoarchean marine sediments before the 3.6 Ga peak in metamorphic conditions.

Implications of the Isua Tourmalines: Possible Roles of Marine Sediments for Chemical Evolution

Geological evidence presented in this study suggests possible boron enrichment in Eoarchean sedimentary environments. Grew et al. (2015) discussed the possibility of boron extraction from the Hadean mantle and concluded that there is no evidence for boron concentrations older than the Isua metasediments; however, it is conceivable that the evidence for boron concentration in the Hadean Earth has not been preserved (or yet discovered). Although the level of boron concentration in the global oceans of the Hadean Earth might have been considerably lower than that of the present ocean (Grew et al. 2015), substantial amounts of boron must have been released into the ocean because of the greater hydrothermal activity at that time (Kakegawa et al. 2002). This would have allowed the attainment of relatively high concentrations of borate within

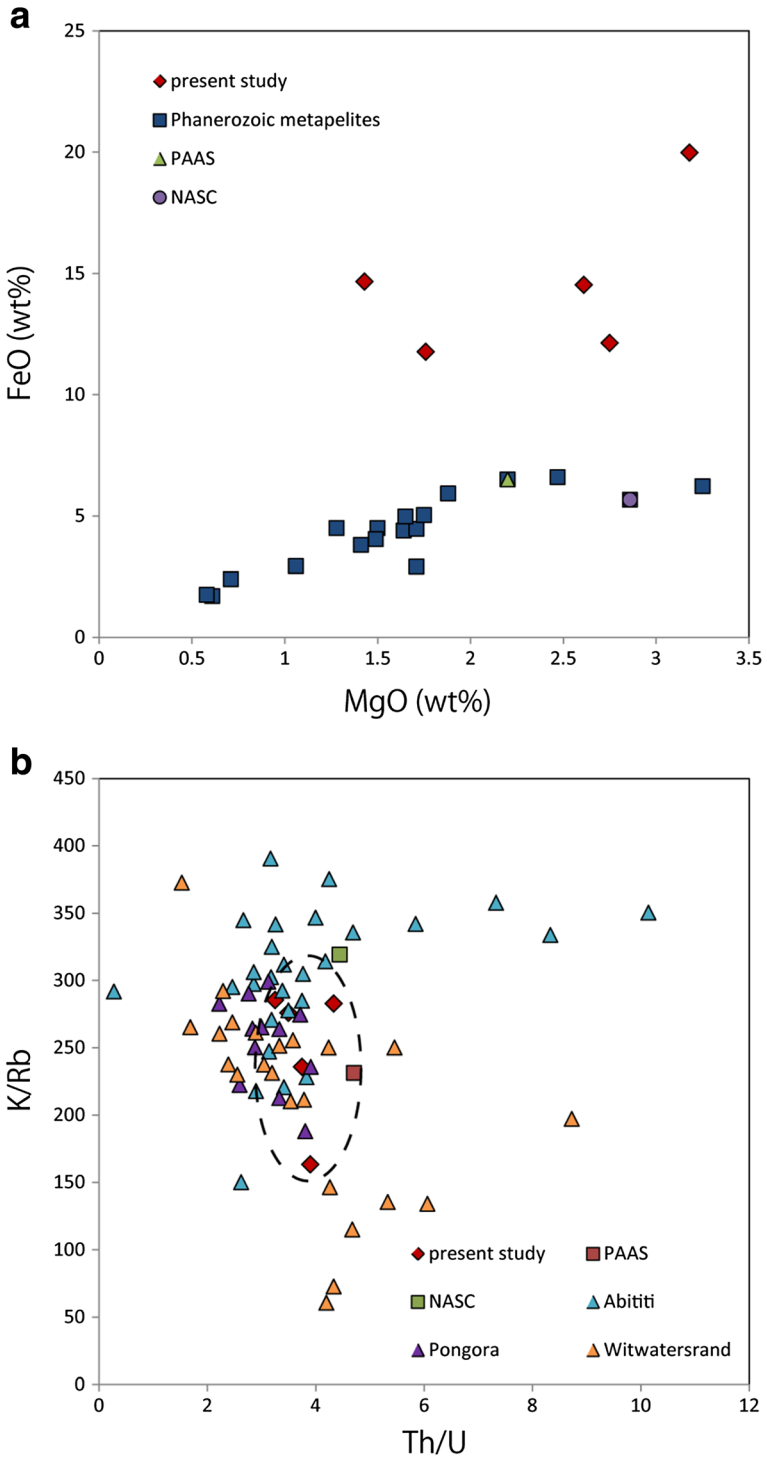
a
present study
Phanerozoic metapelites
PAAS
NASC
FeO (wt%)
MgO (wt%)
0
5
10
15
20
25
0
0.5
1
1.5
2
2.5
3
3.5
b
K/Rb
Th/U
present study
PAAS
NASC
Abititi
Pongora
Witwatersrand
0
50
100
150
200
250
300
350
400
450
0
2
4
6
8
10
12

Table 4 Temperature estimates for Isua metamorphism based on Ferry and Spear (1978)

Pair	$(Mg/Fe)_{Gar}$	$(Mg/Fe)_{Bio}$	K_D	T (°C)
#1	0.0535	0.415	0.129	479
#2	0.0587	0.435	0.135	492
#3	0.0605	0.432	0.14	502
#4	0.0615	0.422	0.146	514
#5	0.0644	0.426	0.151	525
#6	0.0517	0.423	0.122	465
#7	0.0676	0.43	0.157	537
#8	0.0622	0.424	0.147	516
#9	0.0586	0.428	0.137	496
#10	0.0663	0.423	0.157	536
#11	0.0501	0.427	0.117	456
#12	0.0651	0.42	0.155	532
#13	0.0778	0.421	0.185	590
#14	0.0666	0.423	0.158	538
#15	0.055	0.418	0.132	486
#16	0.0607	0.409	0.148	519
#17	0.0761	0.419	0.182	584
Average	0.0621	0.423	0.147	516

local sedimentary environments where clay minerals could have scavenged trace amounts of oceanic boron into the sediments.

In addition, ca. 4.0 Ga metatonalite-trondjemite-granite occurs at Akasta in Canada. Generally, such felsic igneous rocks are important reservoirs of boron (Iizuka et al. 2010). Furthermore, it is proposed that the oxygen isotope compositions of 4.3–4.1 Ga zircons at Jack Hills in Australia formed in Hadean granite via the melting of Hadean marine sediments (Mojzsis et al. 2001). Those Hadean felsic rocks could have been a potential source of borate for the Hadean oceans. Therefore, it is reasonable to assume that borate and organic molecules could have accumulated in marine sediments during the Hadean prebiotic age through processes similar to those of the Eoarchean, when early oceans were in existence (Sleep et al. 2001). On the Hadean Earth, clastic material derived from continental weathering was relatively rare but a considerable amount of silicates, including clays, might have been generated through volcanic activity (Basiuk and Navarro-González 1996), bombardment by meteorites (Cockell 2006), and seafloor weathering. This material could have carried a wide variety of organic molecules, synthesized in space and in the atmosphere, to the seafloor (Chyba and Sagan 1992). Sedimentary processes during the Hadean occurred on top of oceanic crust consisting of mafic to ultramafic rocks, in a sedimentary environment where both borate and organic molecules could have accumulated. As the atmosphere of the primitive Earth contained larger amounts of CO_2 in comparison with the present, the ocean was highly carbonated (Kasting and Catling 2003). This acidic ocean would have been unsuitable for the formose reaction and stabilization of ribose, but fault movements (Hargraves 1986), frequent meteorite impacts (Kring and Cohen 2002) during the Hadean, and/or mud volcanism (Mazzini 2009) might have provided alkaline fluids from underlying serpentinized crust to shallower sedimentary environments. Pore fluids in modern deep marine sediments are alkaline because of the clay buffer effect. Such an effect was most likely also present during the

Table 5 Temperature estimates for Isua metamorphism based on Beyssac et al. (2002)

Sample	Raman shift (cm^{-1})			Height			FWHM			Peak area			R1 (D1/G height ratio)	R2 (D1/(G + D1 + D2) area ratio)	Estimated temperature (°C)
	G	D1	D2	G	D1	D2	G	D1	D2	G	D1	D2			
150114-1	1583	1354	1625	1561	139	31	21	45	12	50334.1	8477.2	396.1	0.0893	0.14	577
150114-2	1583	1352	1626	384	47	10	23	46	13	13045.7	2935.3	143.3	0.1224	0.18	559
150114-7	1583	1352	1623	2451	611	73	22	45	16	81197.6	36363.6	1237.1	0.2493	0.31	503
150114-8	1582	1351	1622	6019	2214	322	25	45	20	213279	129983	6945.7	0.3678	0.38	472
150114-9	1583	1352	1623	816	343	49	23	44	23	29088.5	20789.9	1558.3	0.4203	0.42	456
150114-10	1585	1354	1629	647	151	39	22	43	12	21874.1	8877.2	664.5	0.2341	0.29	513
150114-11	1582	1351	1623	1418	283	26	22	43	14	47095.2	15993.8	385.6	0.1996	0.25	528
150123-1	1584	1353	1624	927	464	90	25	46	20	35026	30254	1958.6	0.5005	0.46	435
Average	1583	1352	1624	1778	532	80	23	45	16	61367.5	31709.2	1661.1	0.2729	0.3	505

Hadean and could have created alkaline pore water conditions with which borate and organic molecules such as ribose might have reacted. Furthermore, it is inferred that a subsequent pH decrease at the water–sediment interface, caused by mixing of alkaline solutions with ambient seawater, made it possible to dissociate borate from its complex with ribose, which should have facilitated further ribose reactions. Thus, taken together with other experimental results, clay-rich environments such as marine sediments might have been plausible sites for the indispensable steps necessary for the emergence of primitive life forms. For example, Fe-oxides, which are common in marine sediments, can catalyze the formation of nucleobase (Shanker et al. 2011). In addition, it has been demonstrated that oligomerization of activated ribonucleotides can be attained on montmorillonite surfaces (Ferris et al. 1996; Ferris 2006), which also catalyzes the formation of vesicles that can incorporate RNA (Hanczyc et al. 2003).

Acknowledgments This study was supported by JSPS General Grant (#24403013). We appreciate Minik Rosing's help with the sample collection. Constructive comments from Edward Grew on the manuscript were helpful to improve this study. We would like to express sincere appreciation to Edward Grew.

Appendix

Garnet–Biotite Geothermometer

The garnet–biotite geothermometer is a method to estimate the temperature experienced by a geologic material, which is based on the temperature dependence of Fe–Mg partitioning between garnet, $Fe_3Al_2Si_3O_{12}$ (almandine)–$Mg_3Al_2Si_3O_{12}$ (pyrope), and biotite, $KFe_3AlSi_3O_{10}(OH)_2$ (annite)–$KMg_3AlSi_3O_{10}(OH)_2$ (phlogopite) at equilibrium following the reaction:

$$Fe_3Al_2Si_3O_{12} + KMg_3AlSi_3O_{10}(OH)_2 = KFe_3AlSi_3O_{10}(OH)_2 + Mg_3Al_2Si_3O_{12}$$
$$\Delta G = \Delta H - T\Delta S + P\Delta V + 3RT\ln K = 0,$$

Where $K=(Mg/Fe)_{garnet}/(Mg/Fe)_{biotite}$ (either on a weight or atomic metal basis).

Values for ΔH, ΔS, and ΔV of this reaction were assessed experimentally by Ferry and Spear (1978) under the condition that these parameters are independent of pressure and temperature. Consequently, the following equation was obtained:

$$12454 - 4.662T(K) + 0.057P(\text{bars}) + 3 \cdot 0.239RT\ln K = 0$$

Graphite Geothermometer

This method is based on the progressive graphitization of carbonaceous grains with increasing temperature, the extent of which can be estimated using Raman spectra. The results of spectral decomposition for all spots, the position and FWHM of the G bands, the D1/G peak intensity ratios (R1) (i.e., peak heights), and the D1/(G + D1 + D2) peak area ratios (R2) are summarized in Table 5. The relationship between the extent of graphitization and temperature can be expressed as follows:

$$T(^\circ C) = -445R2 + 641 \pm 50$$

References

Appel PWU (1995) Tourmalinites in the 3800 Ma old Isua supracrustal belt, West Greenland. Precambrian Res 72(3):227–234

Appel PW, Rollinson HR, Touret JL (2001) Remnants of an early Archaean (>3.75 Ga) sea-floor, hydrothermal system in the Isua Greenstone Belt. Precambrian Res 112(1):27–49

Basiuk VA, Navarro-González R (1996) Possible role of volcanic ash-gas clouds in the Earth's prebiotic chemistry. Orig Life Evol Biosph 26(2):173–194

Benner SA, Kim HJ, Carrigan MA (2012) Asphalt, water, and the prebiotic synthesis of ribose, ribonucleosides, and RNA. Acc Chem Res 45(12):2025–2034

Beyssac O, Rouzaud JN, Goffé B, Brunet F, Chopin C (2002) Graphitization in a high-pressure, low-temperature metamorphic gradient: a Raman microspectroscopy and HRTEM study. Contrib Mineral Petrol 143(1):19–31

Boak JL, Dymek RF (1982) Metamorphism of the ca. 3800 Ma supracrustal rocks at Isua, West Greenland: implications for early Archaean crustal evolution. Earth Planet Sci Lett 59(1):155–176

Bolhar R, Kamber BS, Moorbath S, Whitehouse MJ, Collerson KD (2005) Chemical characterization of earth's most ancient clastic metasediments from the Isua Greenstone Belt, southern West Greenland. Geochim Cosmochim Acta 69(6):1555–1573

Breslow R (1959) On the mechanism of the formose reaction. Tetrahedron Lett 1(21):22–26

Chaussidon M, Appel PWU (1997) Boron isotopic composition of tourmalines from the 3.8-Ga-old Isua supracrustals, West Greenland: implications on the δ 11 B value of early Archean seawater. Chem Geol 136(3):171–180

Chyba C, Sagan C (1992) Endogenous production, exogenous delivery and impact-shock synthesis of organic molecules: an inventory for the origins of life. Nature 355:125–132

Clark CM (2007) Tourmaline: structural formula calculations. Can Mineral 45(2):229–237

Cockell CS (2006) The origin and emergence of life under impact bombardment. Philos Trans R Soc B Biol Sci 361(1474):1845–1856

Danielson A, Möller P, Dulski P (1992) The europium anomalies in banded iron formations and the thermal history of the oceanic crust. Chem Geol 97(1):89–100

Feng R, Kerrich R (1990) Geochemistry of fine-grained clastic sediments in the Archean Abitibi greenstone belt, Canada: implications for provenance and tectonic setting. Geochim Cosmochim Acta 54(4):1061–1081

Ferris JP (2006) Montmorillonite-catalysed formation of RNA oligomers: the possible role of catalysis in the origins of life. Phil Trans R Soc B Biol Sci 361(1474):1777–1786

Ferris JP, Hill AR Jr, Liu R, Orgel LE (1996) Synthesis of long prebiotic oligomers on mineral surfaces. Nature 381:59–61

Ferry JT, Spear FS (1978) Experimental calibration of the partitioning of Fe and Mg between biotite and garnet. Contrib Mineral Petrol 66(2):113–117

Furnes H, de Wit M, Staudigel H, Rosing M, Muehlenbachs K (2007) A vestige of Earth's oldest ophiolite. Science 315(5819):1704–1707

Furnes H, Rosing M, Dilek Y, De Wit M (2009) Isua supracrustal belt (Greenland)—a vestige of a 3.8 Ga suprasubduction zone ophiolite, and the implications for Archean geology. Lithos 113(1):115–132

Furukawa Y, Horiuchi M, Kakegawa T (2013) Selective stabilization of ribose by borate. Orig Life Evol Biosph 43(4–5):353–361

Gilbert W (1986) Origin of life: the RNA world. Nature 319(6055):618

Grew ES, Bada JL, Hazen RM (2011) Borate minerals and origin of the RNA world. Orig Life Evol Biosph 41(4):307–316

Grew ES, Dymek RF, De Hoog JC, Harley SL, Boak J, Hazen RM, Yates MG (2015) Boron isotopes in tourmaline from the ca. 3.7–3.8 Ga Isua supracrustal belt, Greenland: sources for boron in eoarchean continental crust and seawater. Geochim Cosmochim Acta 163:156–177

Gromet LP, Haskin LA, Korotev RL, Dymek RF (1984) The "North American shale composite": its compilation, major and trace element characteristics. Geochim Cosmochim Acta 48(12):2469–2482

Hanczyc MM, Fujikawa SM, Szostak JW (2003) Experimental models of primitive cellular compartments: encapsulation, growth, and division. Science 302(5645):618–622

Hargraves RB (1986) Faster spreading or greater ridge length in the Archean? Geology 14(9):750–752

Hayashi M, Komiya T, Nakamura Y, Maruyama S (2000) Archean regional metamorphism of the Isua supracrustal belt, southern West Greenland: implications for a driving force for Archean plate tectonics. Int Geol Rev 42(12):1055–1115

Henry DJ, Dutrow BL (1992) Tourmaline in a low-grade clastic metasedimentary rock: an example of the petrogenetic potential of tourmaline. Contrib Mineral Petrol 112(2–3):203–218

Henry DJ, Dutrow BL (1996) Metamorphic tourmaline and its petrologic applications. Rev Mineral Geochem 33(1):503–557

Henry DJ, Dutrow BL (2012) Tourmaline at diagenetic to low-grade metamorphic conditions: its petrologic applicability. Lithos 154:16–32
Henry DJ, Guidotti CV (1985) Tourmaline as a petrogenetic indicator mineral - an example from the staurolite-grade metapelites of NW Maine. Am Mineral 70(1–2):1–15
Henry DJ, Novák M, Hawthorne FC, Ertl A, Dutrow BL, Uher P, Pezzotta F (2011) Nomenclature of the tourmaline-supergroup minerals. Am Mineral 96(5–6):895–913
Hoang LH, Hien NTM, Chen XB, Minh NV, Yang IS (2011) Raman spectroscopic study of various types of tourmalines. J Raman Spectrosc 42(6):1442–1446
Holm NG (2012) The significance of Mg in prebiotic geochemistry. Geobiology 10(4):269–279
Holm NG, Dumont M, Ivarsson M, Konn C (2006) Alkaline fluid circulation in ultramafic rocks and formation of nucleotide constituents: a hypothesis. Geochem Trans 7(7):1–13
Iizuka T, Komiya T, Rino S, Maruyama S, Hirata T (2010) Detrital zircon evidence for Hf isotopic evolution of granitoid crust and continental growth. Geochim Cosmochim Acta 74(8):2450–2472
Kakegawa T, Noda M, Nannri H (2002) Geochemical cycles of bio-essential elements on the early earth and their relationships to origin of life. Resour Geol 52(2):83–89
Kasting JF, Catling D (2003) Evolution of a habitable planet. Annu Rev Astron Astrophys 41(1):429–463
Kawakami T, Ikeda T (2003) Boron in metapelites controlled by the breakdown of tourmaline and retrograde formation of borosilicates in the Yanai area, Ryoke metamorphic belt, SW Japan. Contrib Mineral Petrol 145(2):131–150
Keller P, Robles ER, Perez AP, Fontan F (1999) Chemistry, paragenesis and significance of tourmaline in pegmatites of the Southern Tin Belt, central Namibia. Chem Geol 158(3):203–225
Kennedy MJ, Pevear DR, Hill RJ (2002) Mineral surface control of organic carbon in black shale. Science 295(5555):657–660
Kim HJ, Ricardo A, Illangkoon HI, Kim MJ, Carrigan MA, Frye F, Benner SA (2011) Synthesis of carbohydrates in mineral-guided prebiotic cycles. J Am Chem Soc 133(24):9457–9468
Kring DA, Cohen BA (2002) Cataclysmic bombardment throughout the inner solar system 3.9–4.0 Ga. J Geophys Res Planets (1991–2012) 107(E2):4-1
Larralde R, Robertson MP, Miller SL (1995) Rates of decomposition of ribose and other sugars: implications for chemical evolution. Proc Natl Acad Sci 92(18):8158–8160
Leeman WP, Sisson VB (1996) Geochemistry of boron and its implications for crustal and mantle processes. In Boron: Mineralogy, Petrology and Geochemistry in the Earth's Crust, pp. 645–707
Mazzini A (2009) Mud volcanism: processes and implications. Mar Pet Geol 26(9):1677–1680
McDonough WF, Sun SS (1995) The composition of the Earth. Chem Geol 120(3):223–253
Mojzsis SJ, Harrison TM, Pidgeon RT (2001) Oxygen-isotope evidence from ancient zircons for liquid water at the Earth's surface 4,300 Myr ago. Nature 409(6817):178–181
Nakano T, Nakamura E (2001) Boron isotope geochemistry of metasedimentary rocks and tourmalines in a subduction zone metamorphic suite. Phys Earth Planet Inter 127(1):233–252
Nielsen PE (2007) Peptide nucleic acids and the origin of life. Chem Biodivers 4(9):1996–2002
Nutman AP, Bridgwater D (1986) Early Archaean Amitsoq tonalites and granites of the Isukasia area, southern West Greenland: development of the oldest-known sial. Contrib Mineral Petrol 94(2):137–148
Nutman AP, Friend CR, Paxton S (2009) Detrital zircon sedimentary provenance ages for the Eoarchaean Isua supracrustal belt southern West Greenland: juxtaposition of an imbricated ca. 3700 Ma juvenile arc against an older complex with 3920–3760 Ma components. Precambrian Res 172(3):212–233
Nutman AP, Bennett VC, Friend CR, Hidaka H, Yi K, Lee SR, Kamiichi T (2013) The Itsaq Gneiss complex of Greenland: episodic 3900 to 3660 Ma juvenile crust formation and recycling in the 3660 to 3600 Ma Isukasian orogeny. Am J Sci 313(9):877–911
Nutman AP, Bennett VC, Friend CR (2015) The emergence of the Eoarchaean proto-arc: evolution of a c. 3700 Ma convergent plate boundary at Isua, southern West Greenland. Geol Soc Lond, Spec Publ 389(1): 113–133
Ohtomo Y, Kakegawa T, Ishida A, Nagase T, Rosing MT (2014) Evidence for biogenic graphite in early Archaean Isua metasedimentary rocks. Nat Geosci 7(1):25–28
Orgel LE (2004) Prebiotic chemistry and the origin of the RNA world. Crit Rev Biochem Mol Biol 39(2):99–123
Prieur BE (2001) Étude de l'activité prébiotique potentielle de l'acide borique. C R Acad Sci Ser IIc Chem 4(8): 667–670
Ricardo A, Carrigan MA, Olcott AN, Benner SA (2004) Borate minerals stabilize ribose. Science 303(5655):196
Rosing MT (1999) ^{13}C-depleted carbon microparticles in >3700-Ma sea-floor sedimentary rocks from West Greenland. Science 283(5402):674–676
Rosing MT, Rose NM, Bridgwater D, Thomsen HS (1996) Earliest part of Earth's stratigraphic record: a reappraisal of the>3.7 Ga Isua (Greenland) supracrustal sequence. Geology 24(1):43–46

Rudnick RL, Presper T (1990) Geochemistry of intermediate to high-pressure granulites. In Granulites and Crustal Evolution, Springer, Netherlands, pp 523–550
Shanker U, Bhushan B, Bhattacharjee G (2011) Formation of nucleobases from formamide in the presence of iron oxides: implication in chemical evolution and origin of life. Astrobiology 11(3):225–233
Shapiro R (1988) Prebiotic ribose synthesis: a critical analysis. Orig Life Evol Biosph 18(1–2):71–85
Sleep NH, Zahnle K, Neuhoff PS (2001) Initiation of clement surface conditions on the earliest Earth. Proc Natl Acad Sci 98(7):3666–3672
Sutherland JD (2010) Ribonucleotides. Cold Spring Harb Perspect Biol 2(4):a005439
Taylor SR, McLennan SM (1985) The continental crust: its composition and evolution. Blackwell
Tracy RJ, Robinson P (1976) Garnet composition and zoning in the determination of temperature and pressure of metamorphism, central Massachusetts. Am Mineral 61:762–775
Trumbull RB, Krienitz MS, Gottesmann B, Wiedenbeck M (2008) Chemical and boron-isotope variations in tourmalines from an S-type granite and its source rocks: the Erongo granite and tourmalinites in the Damara Belt, Namibia. Contrib Mineral Petrol 155(1):1–18
Williams LB, Hervig RL, Hutcheon I (2001) Boron isotope geochemistry during diagenesis. Part II. Applications to organic-rich sediments. Geochim Cosmochim Acta 65(11):1783–1794
Williamson BJ, Spratt J, Adams JT, Tindle AG, Stanley CJ (2000) Geochemical constraints from zoned hydrothermal tourmalines on fluid evolution and Sn mineralization: an example from fault breccias at Roche, SW England. J Petrol 41(9):1439–1453
Wronkiewicz DJ (1989) Geochemistry and provenance of sediments from the Pongola Supergroup, South Africa: evidence for a 3.0-Ga-old continental craton. Geochim Cosmochim Acta 53(7):1537–1549
Wronkiewicz DJ, Condie KC (1987) Geochemistry of Archean shales from the Witwatersrand Supergroup, South Africa: source-area weathering and provenance. Geochim Cosmochim Acta 51(9):2401–2416